ENGINEERING RESEARCH INSTITUTE
THE UNIVERSITY OF MICHIGAN
ANN ARBOR

Final Report

BRILLOUIN ZONE THEORY AND PHOTOGRAPHIC LATENT-IMAGE STUDIES

George B. Spence
Robert L. Martin
J. H. Enns

Ernst Katz
Project Supervisor

Compiled by J. H. Enns

Project 2158

SOLID STATE SERVICES DIVISION, U. S. AIR FORCE
OFFICE OF SCIENTIFIC RESEARCH
AIR RESEARCH AND DEVELOPMENT COMMAND
CONTRACT NO. AF 18(600)-750
PROJECT NO. R-355-40-10

March 1957

INTRODUCTION

This is the final report dealing with three phases of investigation covered by the contract at the time of termination, October 31, 1956. They are as follows:

Part I: "An Investigation in the Zone Theory of the Energy of Electrons in Metals." This work was reported in detail as a Technical Report (No. 2158-7-T) in August, 1956. It also served as doctoral thesis for the author, George B. Spence. Page 1

Part II: "Results of Investigation of Low-Intensity Reciprocity Law Failure." A detailed report of this investigation was submitted as a Technical Report (No. 2158-5-T) in August, 1956. It too served as doctoral thesis for its author, Robert L. Martin. Page 4

Part III: "The Photographic Sequence Exposure Experiment." This phase of the investigation has not been reported in a formal technical report. The work, however, has been compiled and submitted for publication in the Journal of the Optical Society of America, by the authors, J. H. Enns and E. Katz. Page 8

In the present final report Parts I and II are limited by reproducing only the abstract and table of contents from the original. Part III is included in its entirety, since it has not been reported and distributed previously.

OBJECTIVES

Part I

A theoretical study of Brillouin zones, with special regard to the question of the appearance of energy gaps, is undertaken. It has a bearing on the Jones—Hume-Rothery theory of the physical properties of binary substitutional alloys.

Part II

This investigation is part of a plan to check the consequences of theories of the photographic latent-image formation, with a view toward finding the number of atoms necessary to form a developable speck of latent-image silver. Specifically, the present study deals with the dependence of low-intensity reciprocity failure on grain size, other factors being unchanged.

Part III

This investigation is part of a plan to check the consequences of theories of the photographic latent-image formation, with a view toward finding the number of atoms necessary to form a developable speck of latent-image silver. Specifically, this investigation is based on the order principle which rests on the hypothesis that for isodense exposures the probability of rendering the last grains developable must be equal. This investigation utilizes isodense data obtained from the sequence exposure experiment.

DISTRIBUTION LIST

Agency	No. of Copies
Commander Hq. AF Office of Scientific Research Washington 25, D. C. ATTN: SRQB	5
Commander Wright Air Development Center Wright-Patterson Air Force Base Ohio	
ATTN: WCRRH	1
ATTN: WCRRL	1
ATTN: WCRTL	1
ATTN: WCRTM-1	1
Commander Air Force Cambridge Research Center L. G. Hanscom Field Bedford, Massachusetts	
ATTN: Technical Library	1
ATTN: CRRF	1
Commander Rome Air Development Center Griffiss Air Force Base Rome, New York ATTN: Technical Library	1
Director, Office for Advanced Studies Air Force Office of Scientific Research P. O. Box 2035 Pasadena 2, California	1
Commander European Office, ARDC c/o American Embassy Brussels, Belgium	1
Superintendent Diplomatic Pouch Rooms Department of State Washington 25, D. C.	1
Document Service Center Armed Services Technical Information Agency Knott Building Dayton 2, Ohio	10
Director of Research and Development Headquarters, United States Air Force Washington 25, D. C. ATTN: AFDRD-RE-3	1
Department of the Navy Office of Naval Research Washington 25, D. C.	
ATTN: Code 423	1
ATTN: Code 421	1
Officer in Charge Office of Naval Research Navy No. 100 Fleet Post Office New York, New York	1

DISTRIBUTION LIST (Continued)

Agency	No. of Copies
Commanding Officer Naval Radiological Defense Laboratory San Francisco Naval Shipyard San Francisco 24, California	1
Director, Research and Development Division General Staff Department of the Army Washington 25, D. C.	1
Division of Research U. S. Atomic Energy Commission 1901 Constitution Avenue, N.W. Washington 25, D. C.	1
U. S. Atomic Energy Commission Library Branch Technical Information Div., ORE P. O. Box No. E Oak Ridge, Tennessee	1
Oak Ridge National Laboratory Post Office Box P Oak Ridge, Tennessee ATTN: Central Files	1
Brookhaven National Laboratory Upton, Long Island, New York ATTN: Research Library	1
Argonne National Laboratory P. O. Box 299 Lemont, Illinois ATTN: Librarian	1
Ames Laboratory Iowa State College P. O. Box 14A, Station A Ames, Iowa	1
Knolls Atomic Power Laboratory P. O. Box 1072 Schenectady, New York ATTN: Document Librarian	1
National Bureau of Standards Library Room 203, Northwest Building Washington 25, D. C.	1
National Science Foundation 1520 H. Street, N.W. Washington 25, D. C.	1
Director, Office of Ordnance Research Box CM, Duke Station Durham, North Carolina	1
Office of Technical Services Department of Commerce Washington 25, D. C.	1
Commander Western Development Division (ARDC) P. O. Box 262 Inglewood, California ATTN: WDSIT	1
Document Custodian Los Alamos Scientific Laboratory P. O. Box 1663 Los Alamos, New Mexico	1
Arnold Engineering Development Center P. O. Box 162 Tullahoma, Tennessee ATTN: Technical Library	1

DISTRIBUTION LIST (Concluded)

Agency	No. of Copies
Commanding Officer Ordnance Materials Research Office Watertown Arsenal Watertown 72, Massachusetts	1
Commanding Officer Watertown Arsenal Watertown 72, Massachusetts ATTN: Watertown Arsenal Laboratories Technical Reports Section	1
National Advisory Committee for Aeronautics 1512 H. Street, N.W. Washington 25, D. C.	1

BIBLIOGRAPHICAL CONTROL SHEET

1. Originating agency and/or monitoring agency:

   O.A.: Engineering Research Institute, The University of Michigan
   M.A.: Solid States Sciences Division, Office of Scientific Research

2. Originating agency and/or monitoring agency report number:

   O.A.: ERI Report No. 2158-8-F
   M.A.: AFOSR-TR-57-22

3. Title and classification of title: Brillouin Zone Theory and Photographic Latent-Image Studies (UNCLASSIFIED)

4. Personal authors: George B. Spence, Robert L. Martin, J. H. Enns, and Ernst Katz

5. Date of report: March 1957

6. Pages: 29 + 7 preliminary

7. Illustrative material: 5 figures, 2 tables

8. Prepared for Contract No.: AF 18(600)-750

9. Prepared for Project Code and/or No.: R-355-40-10

10. Security classification: UNCLASSIFIED

11. Distribution limitations: See Distribution List

12. Abstract: The three abstracts for Parts I, II, and III are on pages 1, 4, and 8, respectively.

PART I

AN INVESTIGATION IN THE ZONE THEORY OF THE ENERGY OF ELECTRONS IN METALS

George B. Spence

ABSTRACT

This work is a theoretical investigation of certain general problems which occur in using the zone theory of the electron energy bands to determine the phase boundaries of those alloys agreeing with the Hume-Rothery electron concentration rules. There are four main objectives of the work.

The first objective pertains to the possible existence of an energy gap at an electron concentration corresponding to the volume of the zone, often called the Brillouin zone, of an alloy structure. It is shown that an energy gap cannot exist for some zones because of what is here called a shape degeneracy. Shape degeneracies exist in those zones which cannot be constructed from an integral number of mappings of the unit cell of the reciprocal lattice of the alloy structure. A "mapping" of the unit cell is the division of the unit cell into sections, if necessary, and the translation of each section by a reciprocal lattice vector. Shape degeneracies exist, for example, in the zones of the γ-brass and β-manganese structures.

The second objective is to obtain qualitative information about the energy surfaces in large zones by the correct use of the nearly-free-electron approximation. The main result here is that the electron energy surfaces in some large zones, for example, the γ-brass zone, are not qualitatively similar to the simple surfaces in the first zone of the conduction electrons of the noble metals.

Because of the existence of shape degeneracies and the necessarily complicated nature of the energy surfaces in certain large zones, the volume of these zones cannot, as has been assumed up to now, be used to predict precisely the location of energy gaps or low dips in the density of states.

The third objective is to solve accurately two simple numerical problems. The two- and three-dimensional problems are constructed from two one-dimensional Schrödinger equations with potentials of one and two cosine terms, respectively. The two-dimensional energy contours illustrate some of the complexities of the electron energies which occur in large zones. Accurate density-

of-states functions N(E) for the three-dimensional problems illustrate the type of structure which can occur in these functions and also show the effect on these functions of Brillouin zone planes, corresponding to weak cosine terms, which cut inside the large zone.

The fourth objective is to gain a better qualitative interpretation of the Hume-Rothery rules. The usual approximation is made that the change in the thermodynamic free energy with electron concentration n is due only to the change in the total conduction electron energy U(n). It is shown that for typical phase boundary problems $U_1(n)$ for phase one, instead of increasing relative to $U_2(n)$ as the zone is filled beyond the peak in $N_1(E)$, continues to decrease relative to $U_2(n)$ until that energy is reached at which the total number of electrons are equal in the two phases. This shows that the positions of the phase boundaries cannot be accurately predicted theoretically from the electron concentration corresponding to the peak in the density of states.

Other results of this investigation suggest that N(E) and U(n) are determined primarily by the geometrical shape of the zone and hence should be about the same for different alloys with the same structure. It follows from this that the same phases of the different alloy systems should occur at the same electron concentrations.

TABLE OF CONTENTS

PART II

RESULTS OF INVESTIGATION OF LOW-INTENSITY RECIPROCITY LAW FAILURE

Robert L. Martin

ABSTRACT

The physical properties of the photographic emulsion, the nature of the photographic latent image, the Mott and Gurney theory of latent-image formation, and a simple model used by Webb to calculate an effective electron trap depth are briefly described. This "single-trap-depth" model predicts a simple, isodense, low-intensity reciprocity-law-failure (rlf) curve whose slope rapidly approaches -1 with decreasing intensity of exposure. A quantitative theory of the mechanism of latent-image formation proposed by Katz (outlined in Chapter II) predicts noninteger low-intensity rlf slopes when an exponential distribution of trap depths is assumed, and therefore agrees better with experimental results. It is shown in Chapter V that for this model the limiting slope will also become -1 for sufficiently low intensities (depending on the total number of traps per grain) but the slope for an extended intermediate section is still inversely proportional to the spread in the assumed exponential distribution. This dependence of rlf slope on spread of trap depths suggests that if their distribution varies with grain size, then a relationship between grain size and rlf slope might be expected. This provides the motivation for the experiments described in Chapters III and IV.

A new type of apparatus for use with very low intensities and long times of exposure is described in detail. The principal advantages of this design were the compactness permitted by the use of slides instead of a sector wheel, the simultaneous exposure of three plates, and the flexibility possible with the automatic timing circuit which controlled the exposure program.

Pure AgBr emulsions were used for the experiments of rlf vs grain size in order to avoid difficulties arising from the correlation between iodide content and grain size. Since the characteristics of these emulsions change more rapidly with time than those of ordinary commercial emulsions, a uniform program of storage before and after exposure was employed, with test experiments to demonstrate the validity of this procedure.

The rlf slopes from the five pure AgBr emulsions, whose average grain size ranged from about .2 μ^2 to 5 μ^2, demonstrate a definite increase in slope with average grain size of emulsion used when developed with internal developer and a similar but less marked tendency with surface development. This effect

was stronger when higher temperatures of storage and exposure were used. A systematic indication of more structure in the experimental curves than could be accommodated by either the "exponential-trap-depth" or "single-trap-depth" model was observed. However, this was only slightly beyond the estimated experimental error.

It is shown that a simple model assuming two discrete trap depths provides low-intensity rlf curves of considerable structure which are qualitatively similar to experimental curves. For example, they show an extended, almost straight section of noninteger slope. These curves are described in terms of the relative abundance and depths of deep and shallow traps in the grain. A method of obtaining these parameters by analysis of experimental curves is given.

Suggestions for improvement of the experimental technique and possible additional experiments suggested by the "two-trap-depth" model are offered.

TABLE OF CONTENTS

PART III

THE PHOTOGRAPHIC SEQUENCE EXPOSURE EXPERIMENT

J. H. Enns and E. Katz

ABSTRACT

An instrument is described which has been built for the automatic recording of sequence exposures on 4-by-10-in. photographic plates. Twelve shutter slides are independently timed so that on one plate up to 384 4-by-5-mm rectangles can be uniformly exposed to high and low-intensity radiation. The present design is for an intensity ratio of 100:1, where both intensities are below optimum. With minor modifications the instrument can be converted to operate at other intensity ratios. The densitometer readings are checked from calibration strip data placed adjacent to the sequence exposures. The corrected data, following conversion to Seidel values, are plotted as families of characteristic curves, with the sequence exposure ratio as the constant parameter. Isodense loop data are read from the curves at the intersection with a line drawn parallel to the exposure axis.

A theoretical discussion of isodense loops is presented which is based on the hypothesis that for isodense exposures the probability of rendering the last grains developable must be equal. It is shown how this method should yield the limiting slope of the low-intensity failure curve, and the minimum number of quanta absorbed by the average grain to become developable. Preliminary results presented here for Eastman Kodak Emulsion Type 33 are within expectation.

TABLE OF CONTENTS

I. INTRODUCTION

The concept that the reciprocity law failure below optimum intensities results from disintegration of the latent image in its initial stages of formation has been supported experimentally by Webb and Evans.[1] One of their experiments was based on the sequence effect, first observed by Weinland.[2] In a sequence exposure the emulsion is given an exposure I_1T_1 followed by an exposure I_2T_2. The first of these may be taken as a fraction p of the total exposure E and the second as a fraction q, where $p + q = 1$.

Now the resulting density D is observed to be one function of E and p for the case when the high-intensity exposure is followed by the low-intensity exposure (H+L), and a different function when this order is reversed (L+H). At the terminal points where $p = 0$ and $p = 1$, the two functions must necessarily coincide. Thus a plot of the two D functions of p (at constant E) forms an isoexposure loop. The experimental data of Webb and Evans were presented in the form of isoexposure loops whose shape supported previous evidence that the disintegration of the latent image, which is responsible for the low-intensity failure, occurs in the early stages of latent-image formation. A second stage is distinguished in which the latent-image speck has become stable but is not yet developable.

More recently a theory on the low-intensity sequence effect has been proposed by Katz,[3] which rests on the hypothesis that for isodense exposures the probability of rendering the last grains developable must be equal. This implies that multigrain densitometer measurements should yield single-grain data. In particular the theory indicates how sequence experiments can be used to obtain information concerning the number of atoms which constitute the stable and the developable latent image. The present experiment was designed to furnish isodense sequence loop data suitable for the investigation of the above theory and therefore the study of latent-image formation.

The instrument described below is made up of twelve shutter systems. Each shutter or slide is timed to expose on one side a series of 16 rectangular plate areas to various times of a given "high" light intensity I_H and subsequently the same areas for various times to a given low light intensity I_L. The other side of each slide gives first the low intensity I_L and subsequently the high intensity I_H exposures to a neighboring series of 16 areas. The intensity I_H is admitted to the plate through an open slot in the slide, while the intensity I_L comes through a slot covered by a filter of suitable transmission. If the timing program is such that the ratio of the two exposure times for any given plate area is equal to the filter transmission I_L/I_H, then the data from each slide would be sufficient to plot an isoexposure loop.* The data from at least four or five slides are required for one isodense loop.

*Though not essential, it is practical to strive to satisfy this condition. See Appendix.

Throughout this paper the exposure E' and intensity I' are considered as quantities incident at the front surface of the emulsion. On the other hand, I not primed is taken as the intensity incident on a grain at some point within the emulsion and E without prime is the total exposure for a particular grain.

II. INSTRUMENTATION

A. MECHANICAL SYSTEM

Figure 1 is a photograph of the main instrument panel viewed from the direction of the light source (back side). The panel is mounted vertically at one end of a six-foot-long light box, with the source at the opposite end. At the top of the panel are mounted 46 microswitches which are actuated by the slides and thereby control the timing pulses going to the 12 rotary switches (G. H. Leland, Inc., Type 29). Each rotary switch is mechanically coupled to its shutter slide by means of a rack and pinion arrangement. At appropriate intervals the teeth were stripped from the rack. Thus a slide moves as a freely falling body through appropriate distances when it is released by the pulsed rotary switch. Weights not shown in the photograph are spring-coupled to the lower end of each slide.

The location of the photographic plate is indicated by the dotted outline in Fig. 1. The plate holder, not visible, is fitted from the front side of the panel.

The 12 shutter slides are shown in different open positions along the center of the panel. They are aluminum strips 17 mm wide and 75 cm long, anodized dull black to minimize stray reflections. Into each slide are cut four 4-by-75-mm openings. These are spaced relative to each other so as to expose both sequence events while the slide moves past the plate. Two of the openings are located adjacent to each other and are covered with a neutral filter (Kodak Wratten Gelatin Filter). The transmission I_L/I_H is of the order .01. Through these the low-intensity exposure is made for both sequence events simultaneously.

Exposures from two adjacent shutter systems are shown in Fig. 2. While these show the general character of the original exposures, some quantitative detail was not preserved in the photographic reproduction. It can be noted, however, that except for the terminal densities which should be equal, the H+L exposures (A) exceed in density the L+H exposures (B). The plate calibration exposures (C) are made at the end of a sequence run, through one of the clear slots following a 5-mm lateral displacement of the plate holder and plate.

B. TIMING PROGRAM

The instrument was planned for an intensity and timing ratio of 100:1. The basic timing system consists of a synchronous motor driving a system of gears and four cams. One cam actuates a microswitch at 1-sec intervals; the second cam activates its switch at 1-1/2-sec intervals; and the third and fourth cams similarly operate switches at 100- and 150-sec intervals, respectively. Slide No. 1 is pulsed at 1- or 100-sec intervals depending on whether it is a high- or low-intensity exposure, and similarly slide No. 2 is operated at 1-1/2- and 150-sec intervals.

In addition each of the four basic pulses drives a 5-level, 52-contact stepping switch (C. P. Clare and Co., Type 52). The levels are wired to transmit pulses at 2, 3, 4, 6, 13, 19-1/2, 26, 39, 52, and 78-sec intervals for the fast program and at 100 times these values for the low-intensity exposures. Slides 3 to 12 are timed by the above stepping switch pulses. The total exposure range of the instrument is given by $\log_2 78 = 6.29$.

An exposure run is started with slide 12 which has the longest program (33 hours). A microswitch in the timing circuit of slide 11 is closed by slide 12 at a later time so that both finish at about the same time. Successive slides are started in this way and therefore all finish at about the same time. Three additional microswitches associated with each slide change the operation from fast to slow time, back to fast time, and stop the exposure at the end of the cycle.

C. LIGHT SOURCE

The light source is a small mercury arc lamp, type 11-SC-RE, made by the R and M Manufacturing Company, Pasadena, California. The advantages of this source are high stability (about ± 1%), low thermal output, and as a low-pressure lamp, a sharp line spectrum for monochromatic separation by filtering.

Immediately in front of the lamp a set of absorption filters (Corning Glass, type 5-74) reduces the radiation to the 436-mμ Hg line. The monochromatic output from this system was determined at the National Bureau of Standards to be 0.14 μw per cm^2 at a distance of 50 cm (3.08×10^{11} quanta per cm^2 per sec). This intensity is reduced to the desired I_H value by means of a diffusion screen and a variable aperture near the source.

A sensitive and stable photomultiplier tube—galvanometer detecting device, with a calibration based on the lamp data from the National Bureau of Standards, serves to measure the radiation intensity at the photographic plate. The full-scale range of the device is variable in steps by a factor of about 500. This is done by changing the multiplier tube dynode supply voltage from about 40 volts to 100 volts per stage.

As stated above, gelatin filters in each slide near the emulsion reduce I_H to I_L for the low-intensity exposure. For the simplest interpretation of data it is desirable to work with an intensity ratio I_H/I_L equal to the time ratio 100:1. However, the commercially prepared D = 2.0 filters used during the present experiments when tested at 436 millimicrons were found to transmit only 0.6 to 0.5% instead of the desired 1%. It meant that the I_H/I_L ratio might be anywhere between 160 to 200, necessitating the application of the correction method outlined in the Appendix. Specially prepared filters have recently been obtained from the Eastman Kodak Company whose transmission ratio is 100:1 to within several percent at 436 millimicrons.

III. PHOTOGRAPHIC TECHNIQUE

A. EMULSIONS AND DEVELOPMENT

In these tests Eastman Kodak Plates, Type 33, have been used almost exclusively. Plates with this emulsion were readily available and, being highly uniform, introduced a minimum of unknowns during the study of instrument performance. All plates were prestored at 68°F for several days, and the exposure temperature was 75°F (± 2°). Exposed plates were then stored at 68°F for a period equal to the longest exposure time before developing.

The processing procedure was to develop in D-19 at 68°F for 5 minutes (unless stated otherwise), stop bath 30 seconds, fix 5 minutes, and wash 10 minutes. The developing, stopping, and fixing solutions were agitated by means of a motor-driven rocker. The plates were slow-dried at room temperature for about 24 hours before reading.

B. PLOTTING OF DATA

A study of uniformly exposed plates revealed an edge effect up to 5% in density. It was also noted that calibration strip densities decreased by varying amounts (up to 10%) with increasing densities of adjacent sequence exposures. For these reasons the sequence exposure densities D were all corrected from adjacent calibration strip data before converting to Seidel[4] functions $S = \log_{10}(10^D - 1)$ for plotting of the characteristic curves shown in Fig. 3. The advantage of plotting Seidel values instead of densities is in extending the straight portion of a characteristic curve at the lower end.

The two sets of curves shown in Fig. 3 represent half the sequence data recorded on a plate. The even-valued m curves have been omitted to avoid cluttering the graphs. Rectangles of the various densities on the plate may be labled by two integers $1 \leq n \leq 12$ and $0 \leq m \leq 15$, indicating the slide number and

the order of exposures of one slide. Exposures on the same line on the plate normal to the direction of slide motion have the same m and therefore the same p value (see Appendix). In the Appendix it is shown that a given slide will not give isoexposures if the I_H' to I_L' ratio is different from the T_L to T_H ratio. For the data presented here, this was the case in that the intensity ratio was 160 compared to the time ratio of 100. This explains why the points from one slide do not fall on a constant log E line passing through the upper point for total I_H' exposure of m = 15.

The data for plotting the isodense loops shown in Fig. 4 were taken from Fig. 3. Since p for the upper curve and q for the lower curve are identical, both are computed numerically in the general case as q_m' according to Equation 11.

C. SINGLE-GRAIN DATA FROM ISODENSE SEQUENCE LOOPS

The theory of isodense loops was the subject of the paper listed under Reference 3. In that paper Equations 14a and 14b were derived to represent the curved portions of a schematic loop (Fig. 3, Reference 3). They were derived by expressing the order principle (i.e., for isodense exposures the probability of rendering the last grains developable must be equal) analytically as $W(E-E_o)$ = constant. W represents the probability that a second photoelectron will be liberated while the first is still "alive." $E-E_o$ in first approximation was assumed to be the number of interquantic times occurring in the exposure interval during which the latent image grows to stable size. The total exposure E and the part E_o, which is required to go from the stable to the just developable stage, are absorbed quanta per average grain to become developable last. Since not all absorbed quanta necessarily contribute to the latent-image speck formation which later initiates development, E and E_o will in general be greater than required to form a single developable speck. The magnitude of this factor will be discussed later.

The original loop equations were derived in first approximation by making two assumptions. First, it was assumed that the number of interquantic times in E was equal to E. Strictly it was shown that the interquantic times are given by $E-1+e^{-E}$, which approaches E for $E \gg 1$, approaches E-1 for intermediate values, and $1/2\ E^2$ for $E \ll 1$. The second assumption was to consider W as a function of I only. It will now be shown that the probability function W needs to be considered as a function of T as well as I for the present experiments. The new W and more exact interquantic times will then be used to derive sequence loop equations based on the order principle.

As previously derived (Equation 4, Reference 3), W is given by

$$W = \int_o^T F(t)\ P(t)\ dt \quad , \qquad (1)$$

where P(t)dt, the probability that an interquantic time lies in the interval between t and t+dt, is again given by $I(1-t/T)e^{-It}dt$. F(t) is the survival function whose hyperbolic form $(1+\lambda t)^{-\alpha}$ approaches $(\lambda t)^{-\alpha}$ for $\lambda t \gg 1$. Since λ, the number of probable escapes per second for a trapped electron, has been estimated[5] to be about 100 at ordinary room temperature, the simpler form for F(t) is here assumed. α is the limiting slope of the low-intensity reciprocity-failure curve to be determined later. With these substitutions followed by a partial integration, W becomes

$$W = \lambda^{-\alpha} I \int_o^T (1-t/T)t^{-\alpha}e^{-It}dt$$

$$= (\lambda T)^{-\alpha}e^{-IT} + (I-\beta/T)\int_o^T t^{-\alpha}e^{-It}dt \quad , \qquad (2)$$

where $\beta = 1 - \alpha$. The integral

$$\int_o^T$$

in (2) takes the form of the gamma function if the upper limit is extended to ∞. This approximation was checked to be valid to within several percent for all practical values of α, I, and T. The final form of W as a function of I and T is then

$$W = (\lambda T)^{-\alpha}e^{-IT} + (1 - \beta/IT)\,(I/\lambda)^{\alpha}\,\Gamma(\beta) \quad , \qquad (3)$$

where the first term on the right is negligible everywhere except in the immediate vicinity of the loop terminal points ($IT < 2$). λ is a constant whose absolute magnitude need not be known since it will cancel anyway. $\Gamma(\beta)$ will also cancel when the exponential term in (3) is ignored.

The general expression relating isodense exposures is now

$$W_1(pE-1+e^{-pE}) + W_2(qE-1+e^{-qE}-E_o) = W_L(E_L-1+e^{-E_L}-E_o) = W_H(E_H-1+e^{-E_H}-E_o), \qquad (4)$$

where the sum of the two terms on the left, representing a sequence exposure, is equated (order principle) to the terminal probability for either all low (L) or all high (H) intensity radiation. As previously stated, the first and second exposures are respectively $pE = I_1T_1$ and $qE = I_2T_2$, where $p+q = 1$.

Substituting for the W's in (4) form (3) and ignoring all exponential terms, the loop equations become

upper branch:

$$\left(1 - \frac{\beta}{pE}\right)(pE - 1) + w\left(1 - \frac{\beta}{qE}\right)(qE - 1 - E_o) = w\left(1 - \frac{\beta}{E_H}\right)(E_H - 1 - E_o), \quad (5a)$$

and lower branch:

$$w\left(1 - \frac{\beta}{pE}\right)(pE - 1) + \left(1 - \frac{\beta}{qE}\right)(qE - 1 - E_o) = \left(1 - \frac{\beta}{E_L}\right)(E_L - 1 - E_o), \quad (5b)$$

where $w = (I_H/I_L)^{\alpha}$. Considering (5a) as a function f(E,p), it can be shown that the reciprocal of the slope S of the log E vs p curve for the upper curve over its central range is given by

$$\frac{1}{S} = \frac{w}{w-1} - p \quad . \quad (6)$$

Figure 5 is a plot of the 1/S vs p data taken from the experimental loops of Fig. 4. Theory and experiment agree in that there should be a straight line portion of slope -1. The lower curve is not useful for this purpose because fluctuations in E_o effectively change the curvature over its middle region. Equation 6 and curves of the type shown in Fig. 5 were used to determine w. The limiting slope α of the low-intensity reciprocity-failure curve was computed from $w = (I_H/I_L)^{\alpha}$.

Obtaining the limiting slope α of the low-intensity reciprocity-failure curves in this way is unique, for it does not require prolonged exposures at very low intensities. We intend to test the validity of this assertion in the future by changing the I_H/I_L ratio.

The next step is to determine E_L, E_H, and E_o in absorbed quanta for the average grain to become developable last. In photographic work of this kind, exposure ratios (not absolute exposures) incident at the emulsion surface are known experimental quantities. Considering as usual that the absorbed ratios are the same, the ratios $a = E_L/E$ and $\epsilon = E_L/E_H$ are also known as shown in Fig. 4. Introducing $\underline{a}$ and $\underline{\epsilon}$ into Equation 5a and collecting terms in powers of E, the upper branch equation becomes

$$E^2\left[p^2 + wp\left(q - \frac{a}{\epsilon}\right)\right] - Ep(1+\beta) + \beta\left[1 + wp(1+E_o)\left(\frac{1}{q} - \frac{\epsilon}{a}\right)\right] = 0 \quad , \quad (7a)$$

and similar for the lower branch equation (5b)

$$E^2[wp^2 + p(q-a)] - E\,wp(1+\beta) + \beta\left[w + p(1+E_o)\left(\frac{1}{q} - \frac{1}{a}\right)\right] = 0 \quad . \quad (7b)$$

It should be noted that E_o, still unknown, appears in both quadratic equations for E. However, in first approximation the E_o term is negligible for values of $p \simeq 0.1$ or less. Since this for the upper branch is near the E_H terminal where pE may be less than 2, the ignored exponential terms become important enough to make (7a) invalid. The numerical values obtained for E_L and E_H, where $E_L = aE = \epsilon E_H$, are therefore considered more reliable when obtained from the lower branch. Of the two solutions for E, only the larger (+) value is significant. In Fig. 4 (D = 1.0) the broken line curve has been drawn through points computed from (7b). The bending away of the experimental curve for values of $p > 0.25$ has been ascribed to fluctuations in E_o.[3] For values of $p < .05$ the exponential terms in (4) should be included for the computation of the theoretical curve.

It is now possible to solve for E_o in terms of E_L and E_H from the terminal exposures. The solution is

$$E_o = \frac{w\left(1 - \frac{\beta}{E_H}\right)(E_H - 1) - \left(1 - \frac{\beta}{E_L}\right)(E_L - 1)}{w\left(1 - \frac{\beta}{E_H}\right) - \left(1 - \frac{\beta}{E_L}\right)} \qquad (8)$$

where again all exponential terms are small and have been ignored.

In Table I, column 1 lists six plates from which the photographic data were taken; column 2 gives the loop density; column 3 the developing time in minutes; column 4 the measured intensity at the emulsion front surface in quanta per cm^2 per sec; columns 5, 6, 7, and 8 give the values for ϵ, a, w, and α derived as outlined above; the last four columns are computed absorbed quanta per average grain to become developable last.

For the computation of the exposure data of Table II, the average grain size of the Type 33 emulsion (first five plates) was estimated as 0.25 μ^2, and of the special emulsion (plate 409) as 1.0 μ^2. I_L' and I_H' are measured front surface incident intensities in quanta per cm^2 per sec, T_L and T_H the corresponding exposure times, and E_L' and E_H' the total incident exposures in quanta per average grain size at the front surface.

D. DISCUSSION OF DATA

The present data should be considered as preliminary. Only runs with conditions of plates 408 and 413 were repeated. These reproduced very well. However, a glance at the overall data indicates that the results from plate 410 are not in order, and need to be repeated. Neglecting plate 10, α, the limiting slope of the low-intensity reciprocity-failure curves, is essentially not affected by changes in intensity nor developing time. This is as expected.

TABLE I

EXPERIMENTAL DATA

(1) Plates	(2) Density	(3) Dev. Time (min)	(4) I_H'	(5) ϵ	(6) a (p = 0.1)	(7) w	(8) α	(9) E (p = 0.1)	(10) $E_L = aE$	(11) $E_H = \frac{E_L}{\epsilon}$	(12) E_o
408	1.0	5	1.7×10^8	3.03	1.173	4.05	0.266	48.2	56.5	18.7	4.8
410	1.0	5	5×10^8	3.05	1.193	4.51	0.297	43.7	52	17	5.7
414	1.0	5	9.4×10^8	2.6	1.114	4.08	0.277	30.9	34.2	13.2	5.0
411	1.0	4	5×10^8	2.81	1.153	4.05	0.276	40.9	47	16.7	5.4
413	1.0	3	5×10^8	2.7	1.165	3.84	0.265	51	59	21.8	7.3
413	0.6	3	5×10^8	2.62	1.141	3.86	0.266	41.1	46.8	17.9	6.4
413	0.3	3	5×10^8	2.53	1.117	3.82	0.264	35	39.2	15.5	5.7
409*	0.3	Int. Dev.	22×10^8	3.92	1.366	4.73	0.296	115	157	40.1	7.2

*Pure AgBr emulsion, minimum sulphur sensitization, internal image developing.

TABLE II

INCIDENT EXPOSURE DATA

Plates	Density	I_L'	I_H'	T_L (min)	T_H (sec)	E_L'	E_H'
408	1.0	8.8×10^5	1.7×10^8	2400	250	317	104
410	1.0	31×10^5	5×10^8	373	45.5	175	57
414	1.0	59×10^5	9.4×10^8	182	26.3	161	62
411	1.0	31×10^5	5×10^8	340	45.5	159	57
413	1.0	31×10^5	5×10^8	412	58	193	72
413	0.6	31×10^5	5×10^8	210	30	98	37
413	0.3	31×10^5	5×10^8	110	16.2	52	20
409	0.3	116×10^5	22×10^8	1253	101	8750	2230

An estimate of the reliability of the computed absorbed quanta in Table I can be made by comparing these data with Webb's[6] results on single-grain-layer emulsions. The emulsion type he used was a non-color-sensitized, low-speed, fine grain (0.275 μ^2), positive-type. His absorbed quanta (independent of wave length) per average grain size came out to be 16 when the ratio of developable to total number of grains per unit area was 0.1. This is comparable to $E_H = 15.5$ in the present experiments for plate 413, D = 0.3. At so low a density it can be assumed that only grains near the surface have been rendered developable. Webb's exposure time was 15 sec compared to $T_H = 16.2$ sec in the present experiment, indicating comparable light intensities.

By statistical analysis Webb[6] obtained for the average grain a factor 0.24 as the ratio of quanta utilized in forming the latent image that initiates development to the total quanta absorbed. If the E_o values of Table I are multiplied by this factor the result is a number of between 1 and 2 for the quanta necessary to bring the latent image from the stable to just developable size. The product 0.24 E_H for the optimum case of plate 413 (D = 0.3) also gives a value between 3 and 4 for the total quanta required to build a developable speck. These figures are in good agreement with the Gurney-Mott theory of latent-image formation.

The values for E_L and E_H, with the possible exception of plate 410, are consistent in that they increase: (a) with decreasing incident radiation, (b) with decreasing development time, and (c) with increasing density. The first effect is expected from reciprocity failure, the second can be considered as a lowering in developing efficiency, and finally the last grains to become developable with increasing density are deeper within the emulsion or smaller so that this also becomes a reciprocity-failure effect. For plate 409 E_L and E_H

are of course much larger due to emulsion type (minimum sensitization) and because of internal image development.

E_o in Table I shows a consistent change mainly for a change in density. But this is small and as yet unexplained. That E_o is a constant, and is essentially the same for the internal image case, is according to theory.

A comparison of the incident exposures E_L' and E_H' of Table II with the absorbed quanta E_L and E_H of Table I is especially of interest for plate 413. For densities $D \to 0$ the values of E_L' and E_H' tend to the same limits as E_L and E_H. This signifies that all quanta incident on a grain are used in the process of latent-image formation, since for low densities the only affected grains lie at the front surface of the plate. For higher densities the loops reflect the behavior of the average grain at average depth. An estimate of the decrease of light intensity between the front and back surfaces permits one to calculate the ratios E_L'/E_L and E_H'/E_H to be expected. These ratios are in qualitative agreement with the results of Tables I and II at the density $D = 1$.

IV. APPENDIX

When the intensity ratio I_H' to I_L' is not the same as the timing ratio T_L to T_H the sequence strips in Fig. 2 are not isoexposures, but vary in total exposure from step to step. The high- and low-intensity parts of the exposures can then be computed for each step as will now be shown.

For the high- followed by the low-intensity exposure (H+L) the total exposure for the m^{th} place behind the n^{th} slide is

$$E'_{n,m} = p_m E'_{n,15} + q_m E'_{n,o} = p_m I_H' T_{H,n} + (1-p_m) I_L' T_{L,n} , \qquad (9)$$

where $p_m E'_{n,15}$ expresses the high-intensity part of the exposure as a fraction p_m of the all-high-intensity exposure for the case $p_m = 1$ (the bottom step $m = 15$ in Fig. 2), and $q_m E'_{n,o}$ represents the low-intensity part of the exposure as a fraction q_m of the all-low-intensity exposure for the case $p_m = 0$ (the top step $m = 0$ in Fig. 2). The design of the apparatus insures that $p_m + q_m = 1$, and setting

$$k = \frac{I_H'}{I_L'} \frac{T_{H,n}}{T_{L,n}}$$

the ratio $T_{H,n}/T_{L,n}$ is independent of n, while the ratio I_H'/I_L' is independent of n for a uniform filter. Equation 9 now becomes

$$E'_{n,m} = I_H' T_{H,n} \left[p_m + \frac{1-p_m}{k} \right] , \qquad (10)$$

where $I_H' T_{H,n}$ is the total exposure for the case $p_m = 1$, the bottom step ($m = 15$) in Fig. 2. The expressions for the values of p_m' and q_m' giving the fraction of the total exposure at each place admitted as high and as low intensity are found as follows.

For the H+L exposures p_m' and q_m' are defined by the relations

$$p_m E'_{n,15} = p_m' E'_{n,m}$$

$$q_m E'_{n,o} = q_m' E'_{n,m}$$

with

$$p_m' + q_m' = 1 .$$

Substituting these relations in Equation 10 yields

$$p_m' = \frac{mk}{15 + m(k-1)}$$

$$q_m' = \frac{15-m}{15 + m(k-1)} \quad . \tag{11}$$

For the L+H exposures the expressions for p_m' and q_m' should be interchanged. For $k = 1$, p_m' and q_m' become equal to $p_m = m/15$ and $q_m = 1 - m/15$, respectively. It is seen that exposures with $k \neq 1$ correspond to the same p_m' for the same values of m. Thus the measured points can be connected by the family of curves shown in Fig. 3. Each curve is characterized by the p' or q' value computed from Equation 11.

All exposures and intensities in this appendix are taken per unit area at the front surface of the photographic plate.

REFERENCES

1. J. H. Webb and C. H. Evans, J. Opt. Soc. Am., 28, 431 (1938).

2. C. E. Weinland, J. Opt. Soc. Am., 16, 295 (1928).

3. E. Katz, J. Chem. Phys., 18, 499 (1950).

4. H. Kaiser, Spectrochim. Acta, 3, 159 (1948).

5. E. Katz, J. Chem. Phys., 17, 1132 (1949).

6. J. H. Webb, J. Opt. Soc. Am., 38, 312 (1948).

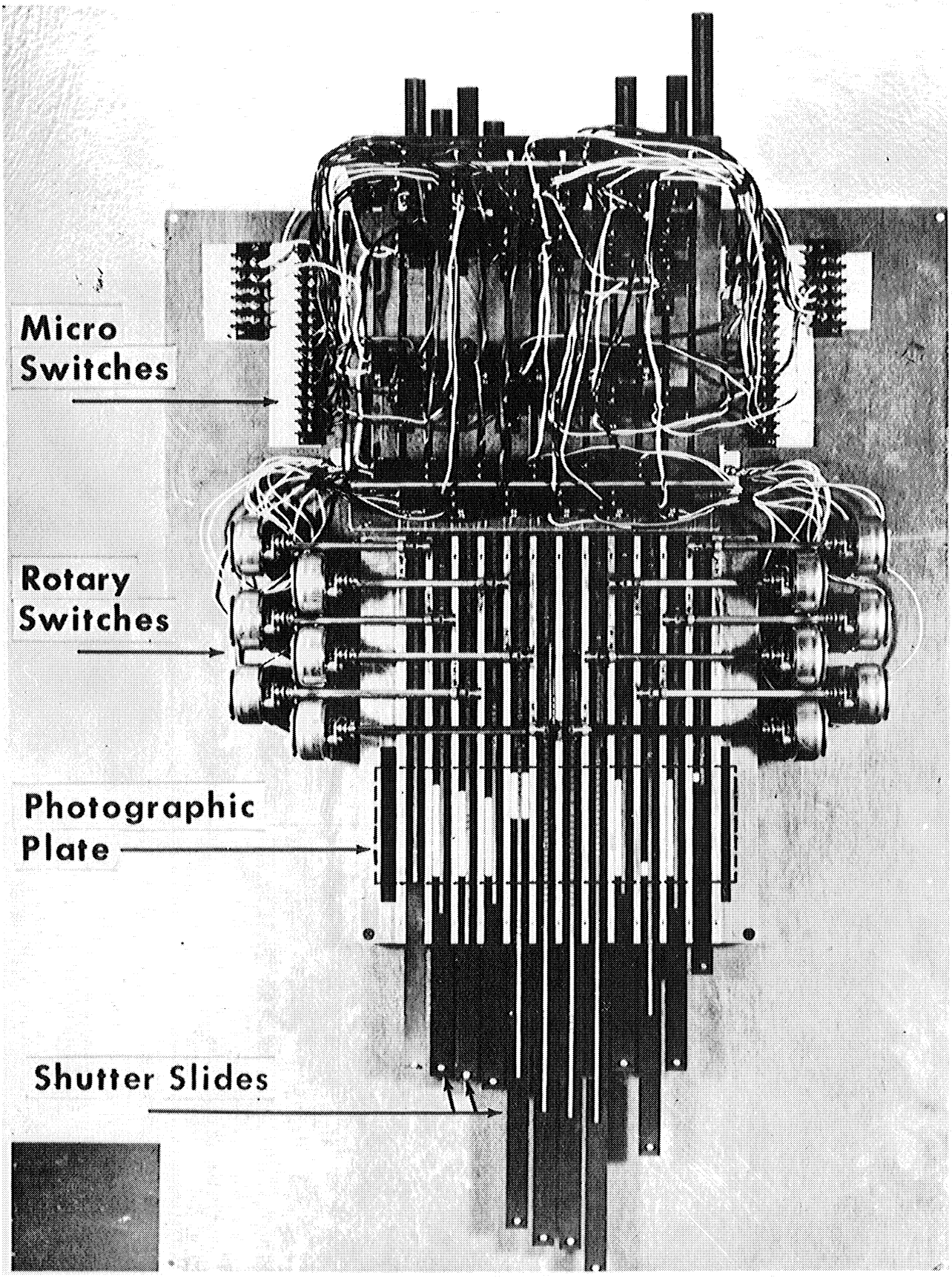

Fig. 1. Sequence exposure instrument panel.

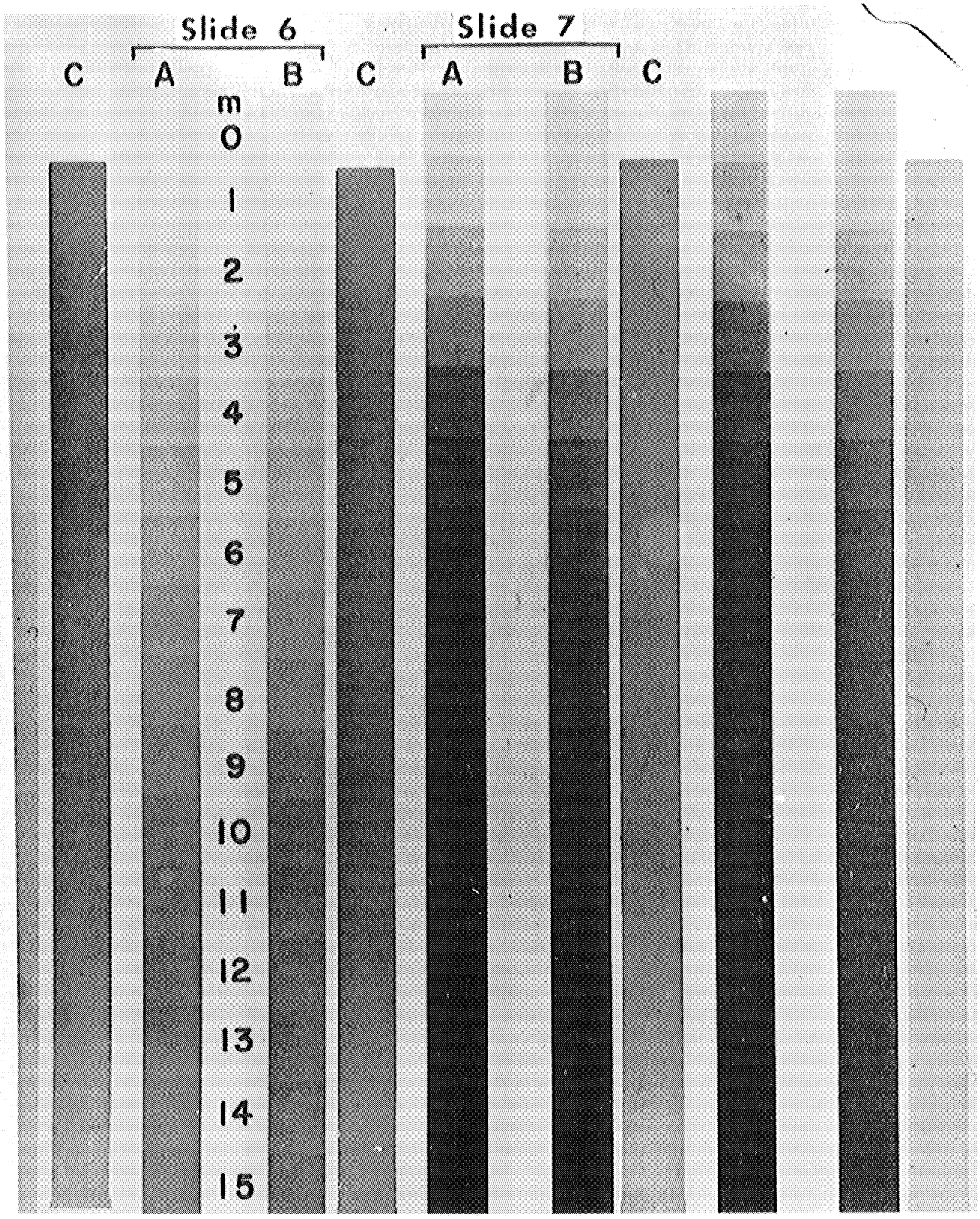

Fig. 2. Sample sequence exposures for two adjacent slides.

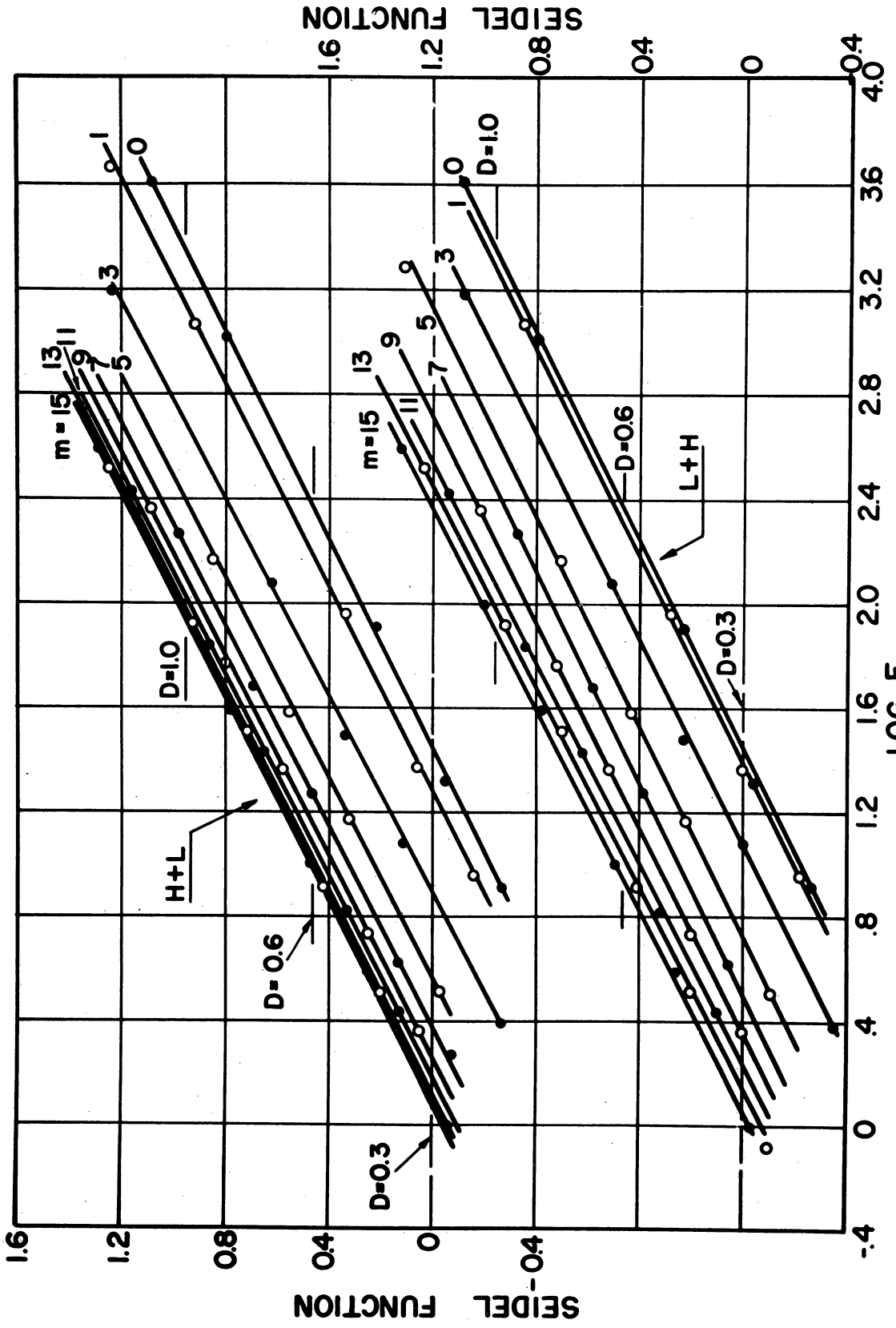

Fig. 3. Typical set of characteristic curves from one plate, with sequence exposure ratio as constant parameter.

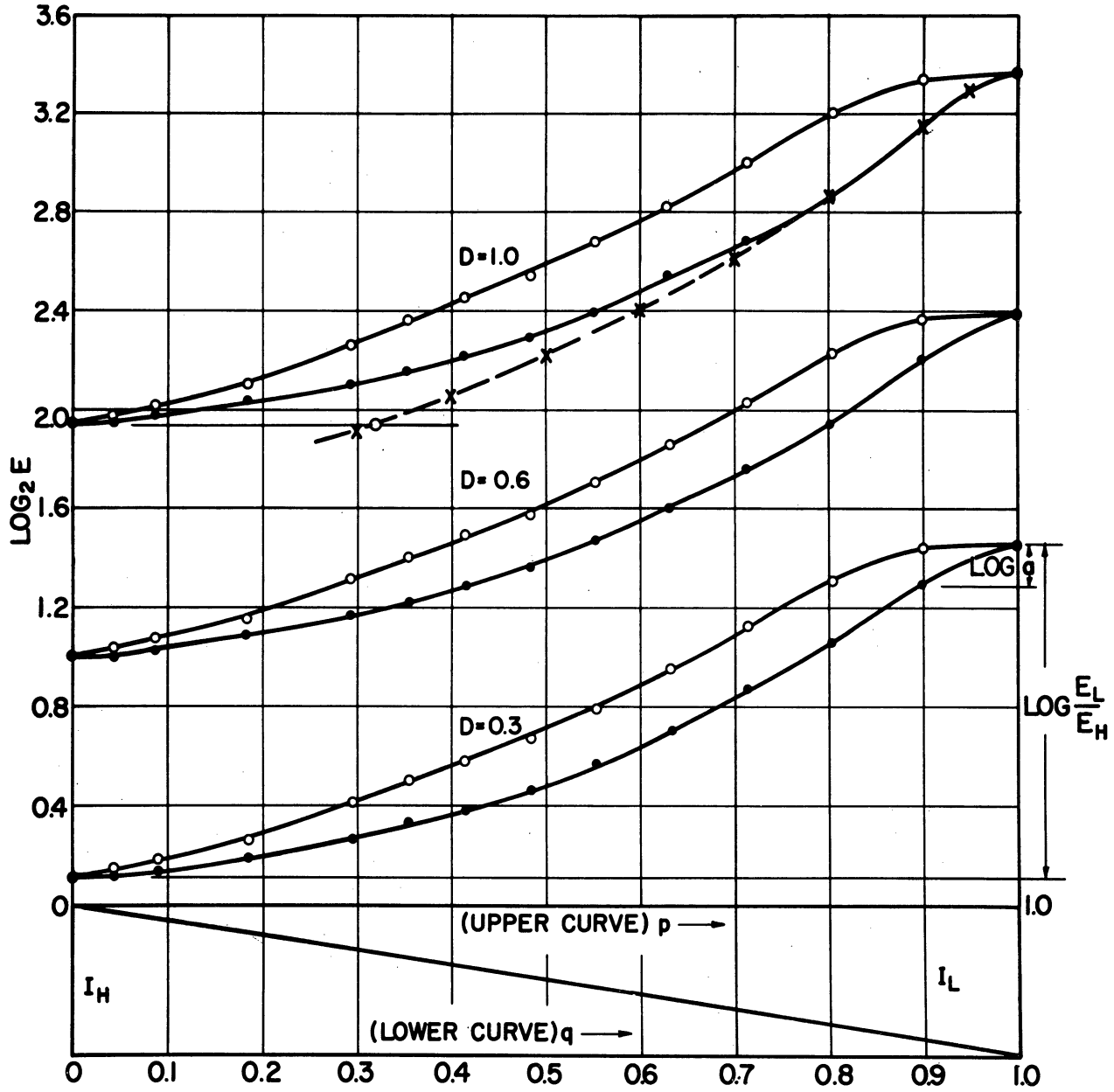

Fig. 4. Typical set of isodense loops, from one plate, for the densities 1.0, 0.6, and 0.3.

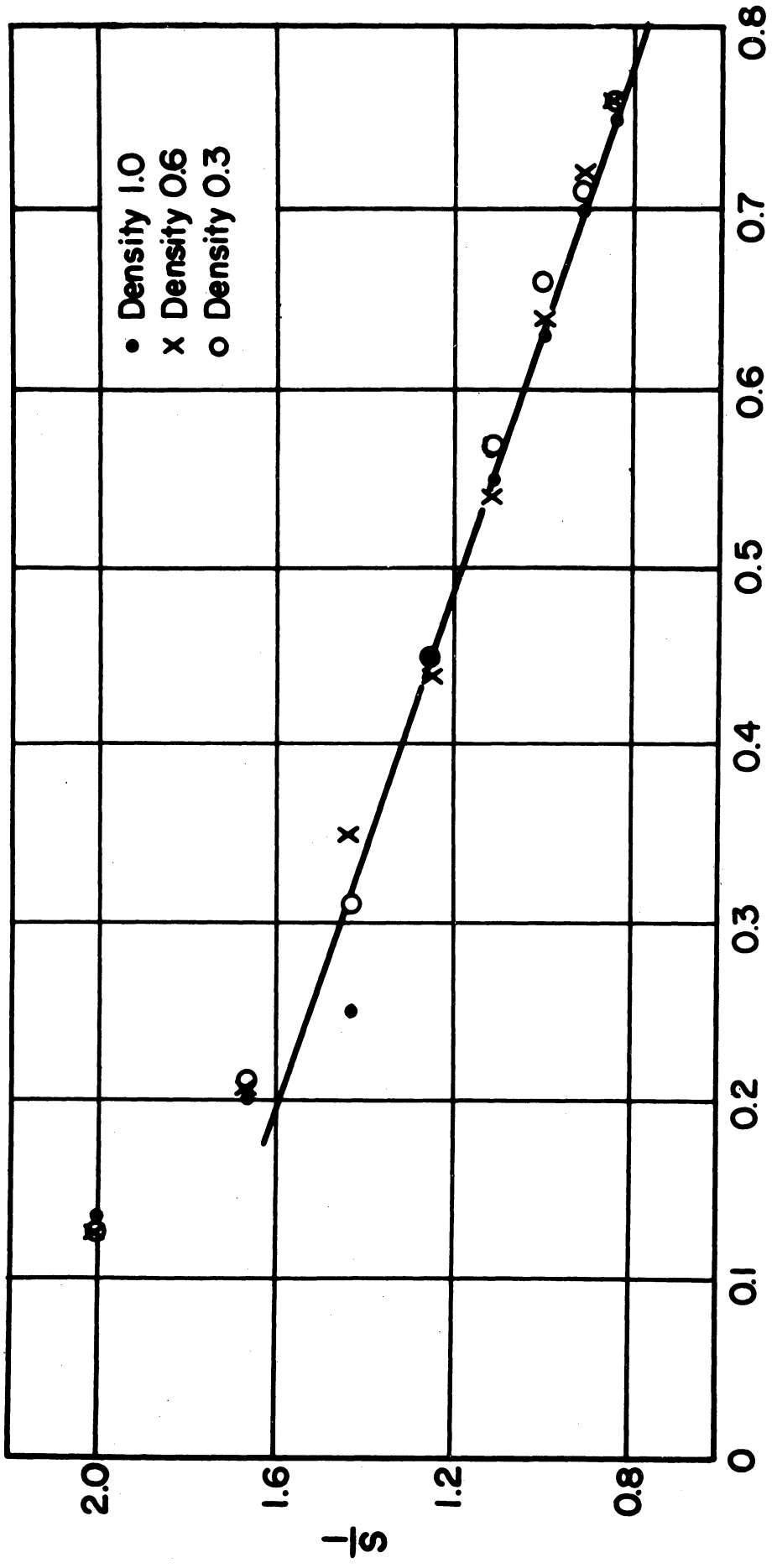

Fig. 5. Experimental data plotted as 1/S vs p for the upper (L+H) curves of each loop in Fig. 4.